Desalination and Water Treatment
www.deswater.com

doi: 10.5004/dwt.2023.30102

314 (2023) 122–129
December

Facile preparation, characterization and photocatalytic properties of barium carbonate nanoparticles

K. Buvaneswari[a], E. Pitchaimani[b], S. Anand[c], R. Arunadevi[d,*]

[a]*P.G. Department of Chemistry, Sri S. Ramasamy Naidu Memorial College, Sattur-626203, Mobile No.: 7904563881; email: buvanasrnmc@gmail.com*
[b]*P.G and Research Department of Chemistry, C.P.A. College, Bodinayakanur, Tamil Nadu, India-625513, Mobile No.: 7639279715; email: pitchaimani06697@gmail.com*
[c]*Entomology Research Institute, Loyola College, Chennai-600034, Tamil Nadu, India, Mobile No.: 7010585017; email: anand.anandsri@gmail.com*
[d]*Department of Chemistry, D.K.M. College for Women (Autonomous), Vellore-632001, Tamil Nadu, India, Mobile No.: 9789683694; email: arunarajan3@gmail.com*

Received 6 July 2023; Accepted 29 October 2023

ABSTRACT

The development of new efficient photocatalysts is critical for a variety of applications including water purification and water splitting. Unfortunately, because TiO_2 has a wide band gap, the photocatalytic applications of TiO_2 NTAs are restricted to light in the ultraviolet (UV) range. Nanosized barium carbonate nanoparticles were prepared by a precipitation method at relatively low temperatures. The prepared samples were characterized by X-ray diffraction, UV-Visible diffuse reflectance spectroscopy, Fourier-transform infrared spectroscopy and scanning electron microscopy with energy-dispersive X-ray spectroscopy techniques. The nanocomposite exhibited a strong photocatalytic activity for decomposition of Crystal violet (CV) under visible light irradiation. The influences of catalyst amount, initial Crystal violet concentrations, pH of the reaction solution and different anions on CV decolorization and degradation reaction kinetics were investigated. The dye could be decolorized more efficiently in acidic media than alkaline media. Furthermore, the photocatalyst indicated phenomenal strength after four response cycles. At last, the conceivable component for the action upgrade was examined in detail.

Keywords: Barium carbonate; Nanoparticles; Crystal violet; Visible light; Photocatalysis

1. Introduction

In the course of recent decades, ecological issues related with destructive natural poisons in squander water are main thrust for supported central and applied exploration in the region of ecological remediation [1]. As of late, much color containing wastewater was created in material, paper, and printing enterprises. Colors are commonly truly stable to light and oxidation because of the complex fragrant atomic structures, yet this makes harm the earth and significantly compromises human wellbeing [2–4]. Along these lines, the viable treatment of this wastewater is one of the most urgent issues before discharging them into nature. Up to this point, different procedures have been investigated to expel the colors from wastewater, including adsorption [5], photodegradation [6], flocculation [7], electrolysis [8], and biodegradation [9]. Adsorption and photograph corruption are viewed as the most serious methods among these applications, since they have the benefits of minimal effort, high productivity, and condition well disposed. The revealed

* Corresponding author.

adsorbents [10,11], for example, zeolite, enacted carbon, share for all intents and purpose the huge surface territory and physical and concoction security. Then again, various semiconductors have been utilized as photocatalysts for the color evacuation [12–14]. Be that as it may, the color evacuation effectiveness by adsorbents depends on their ability and explicit surface regions. The photodegradation productivity primarily relies upon the photocatalytic exercises of photocatalysts, which is generally upset by the agglomeration of the ultrafine powders. The mix of photodegradation with adsorption technique ought to be one of the most encouraging approaches to improve the color expulsion productivity, that is, participating the photocatalysts on adsorbents without yielding their permeable properties.

Semiconductor photocatalysts have pulled in much consideration, due to their possible applications in the remediation of ecological toxins. Photocatalysts can debase contaminations into little inorganic atoms. This synthetic remediation procedure is worthwhile because it is naturally agreeable, requires low response temperatures, and is exceptionally steady. Photocatalysts can likewise be utilized for sun-oriented vitality applications [15–19]. Until this point in time, the specialists are a lot of quick to create different semiconductor materials, for example, TiO_2 [20], ZnO [21], $SrTiO_3$ [22], WO_3 [23], CdS [24], GaN [25], $BiVO_4$ [26], $NaBiO_3$ [27], Ag_3PO_4 [28], CeO_2 [29], Bi_2S_3 [30] and Fe_2O_3 [31], for degradation of different colors [32].

Most of the rare earth oxalates and carbonates have wide applications in electro-optical gadgets and a few applications in industry for delivering barium salts, shades and barium ferrite. Barium carbonate ($BaCO_3$) is likewise utilized as a forerunner for delivering superconductor and earthenware materials and other significant applications in optical glass and electric condensers. Few researchers used $BaCO_3$ nanoparticles with TiO_2, g-C_3N_4 and SnO_2 [33,34] etc., Among all Metal carbonates are the post prominent catalysts for their applied as photocatalysts to treat the wastewater. $BaCO_3$ has shown considerable potential in recent years due to its unique characters such as its low cost, oxidation potential, photosensitivity, acceptable photocatalytic performance and high chemical stability etc., unlike the bulk materials, $BaCO_3$ have a definite surface area which is having a critical responsibility in the generation of photogenerated charge carriers and reactive oxygen species such as hydroxyl radicals which enable pollutant adsorption and mineralization when treated with ultraviolet (UV) light. To the best of our knowledge there is no report about photocatalytic activity of Crystal violet using $BaCO_3$ nanoparticles and our catalyst have 91% of removal efficiency.

Henceforth, this examination meant to blend barium carbonate photocatalysts with an easy precipitation strategy. Various instruments including X-ray diffraction (XRD), energy-dispersive X-ray spectroscopy (EDX), scanning electron microscopy (SEM), Fourier-transform infrared spectroscopy (FT-IR) and UV-Visible diffuse reflectance spectroscopy (UV-Vis DRS), were applied to portray them in detail. The photocatalysts were utilized to corrupt precious stone violet under noticeable light illumination. After examination the impact of different boundaries of $BaCO_3$ nanoparticles likewise considered. Furthermore, the photocatalyst indicated phenomenal strength after four response cycles. At last, the conceivable component for the action upgrade was examined in detail.

2. Materials and methods

2.1. Materials

All the chemicals used in this experiment were of analytical grade purchased from Merck Chemicals (India). Double distilled water was used throughout the experiments.

2.2. Experiment

2.2.1. Preparation of barium carbonate

The $BaCO_3$ (BCO) nanoparticles were prepared by simple co-precipitation method. Barium chloride ($BaCl_2$) was used as starting materials. Typically, 5 g of barium chloride ($BaCl_2$) and 1 g of citric acid ($C_6H_8O_7$) was dissolved in 50 mL of distilled water. The obtained solution was continuously stirred mean while NH_4OH solution was added until complete precipitating (solution pH value 7) obtained. After stirring for another 3 h the precipitate was filtered and washed thoroughly with distilled water finally the precipitate was dried at 100°C for 1 h and calcinated at 450°C for 3 h.

2.2.2. Measurement of photocatalytic activity

Photocatalytic tests were done in an inundation type photoreactor. 300 mL of Crystal violet with an underlying grouping of 10 μM was taken in a round and hollow glass vessel, which was encircled by a flowing water coat to cool the light. Air was foamed ceaselessly into the aliquot by an air light so as to give a steady wellspring of broke up oxygen. Before light illumination the response blend was mixed in dim for 30 min to accomplish the adsorption–desorption harmony between the impetus and color particles. A 300 W Xe circular segment light with a bright cut off channel was utilized as the noticeable light illumination source. Over the span of light illumination, 5 mL of aliquot was gathered at ordinary time timespan min. At that point the examples were centrifuged to expel the photocatalyst and the filtrate was broke down by UV-obvious spectrometer at λ_{max} = 588 nm. The photodegradation of gem violet was determined by the recipe given underneath.

$$\text{Photodegradation}(\%) = \frac{C_0 - C}{C_0} \times 100 \quad (1)$$

where C_0 is the concentration of Crystal violet before irradiation time and C is the concentration of crystal after a certain irradiation time.

3. Results and discussion

3.1. UV-Visible diffuse reflectance spectroscopy

The optical properties of the nanoparticles are very essential factor for determining their photolytic efficiency. Fig. 1 shows the UV-Vis DRS spectra of BCO. The optical band gaps were analyzed by Tauc equations:

$$\alpha = \frac{C\left(h\nu - E_g^{\text{bulk}}\right)^2}{h\nu} \quad (2)$$

where α, *C*, *hυ* and E_g^{bulk} are absorption coefficient, constant, photon energy and band gap, respectively. Generally, the highest photocatalytic activity is due to the narrow band gap. Tauc plots of BCO are depicted in Fig. 2. The band gaps of BCO was found to be 3.3 eV. The narrow band gap of BCO nanoparticles possesses excellent visible light photocatalytic activity than bare barium carbonate.

3.2. X-ray diffraction

The phase identification of the BCO nanoparticles was performed using XRD (Fig. 3). All diffraction peaks were identified to be orthorhombic $BaCO_3$-compared to the JCPDS No. 05-0378 (*a* = 5.3140 Å, *b* = 8.9040 Å, and *c* = 6.4300 Å, and α = β = λ = 90°) slightly broadened diffraction peaks with 2θ of 19.54, 23.99, 27.68, 29.71, 34.32, 39.62, 42.42, 44.28, 44.98, 55.70, and 56.15 as the (110), (111), (002), (012), (130), (220), (221), (202), (132), (241), and (151) planes for $BaCO_3$, respectively. The average crystalline size of the powders was measured by X-ray line-broadening technique of XRD peaks, using the Scherrer's formula:

$$d_{\text{XRD}} = \frac{K\lambda}{\beta\cos\theta} \quad (3)$$

where θ is the Bragg angle of diffraction lines, *K* is a shape factor taken as 0.9, λ is the wavelength of incident X-rays (λ = 0.154056 nm), and β is the full width at half maximum (FWHM). The size of the nanoparticles was found to be 38 nm.

3.3. Fourier-transform infrared spectroscopy

The spectra of unadulterated BCO nanoparticles after calcination were recorded utilizing JASCO FT-IR Spectrometer with a goal of 4 cm^{-1}, in the scope of 400 to 4,000 cm^{-1}. FT-IR spectra of $BaCO_3$ have been concentrated to decide the impact of surfactant on the microstructure of nanocrystals. It was discovered that citric corrosive and water/oil interface have no impact on the microstructure of $BaCO_3$.

3.4. Scanning electron microscopy with energy-dispersive X-ray spectroscopy

The size and morphological study of the barium carbonate nanoparticles were carried out using the SEM image. The typical SEM images of the $BaCO_3$ powders are shown in Fig. 5. As shown in this image, $BaCO_3$ consisted of irregular plate-like morphology and rough agglomerated particles. Fig. 6. shows the EDX spectra of synthesized BCO nanoparticles. From the figure it shows the BCO containing Ba, C, O in their normal KeV values.

3.5. Evaluation of photocatalytic activity of BCO

The photocatalytic activity of BCO nanoparticles are shown in Fig. 7. The Crystal violet (CV) photodegradation on the samples follows the pseudo-first-order kinetics model:

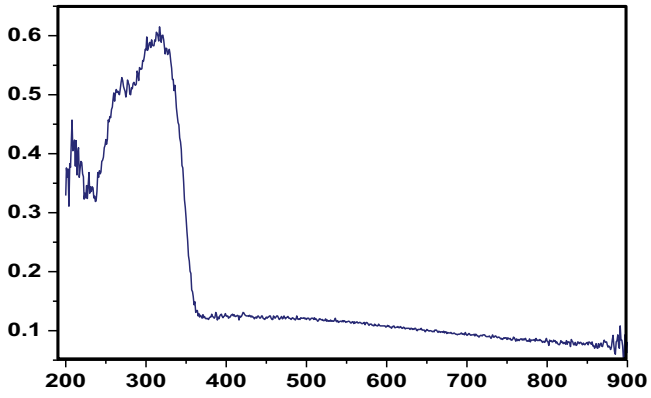

Fig. 1. UV-Visible diffuse reflectance spectra of BCO.

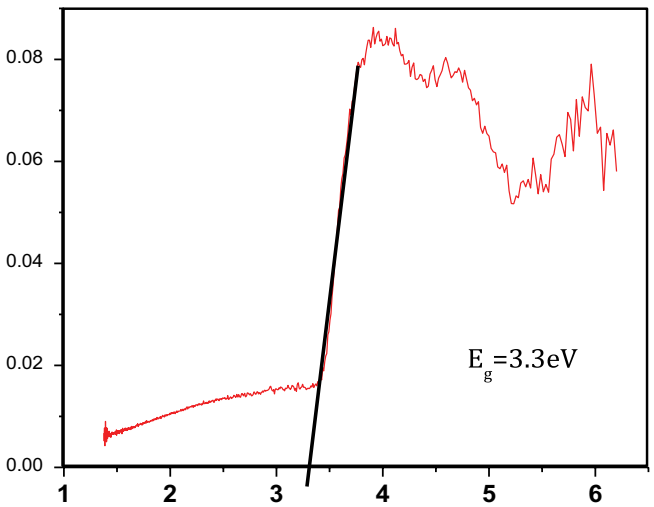

Fig. 2. Tauc plot of BCO.

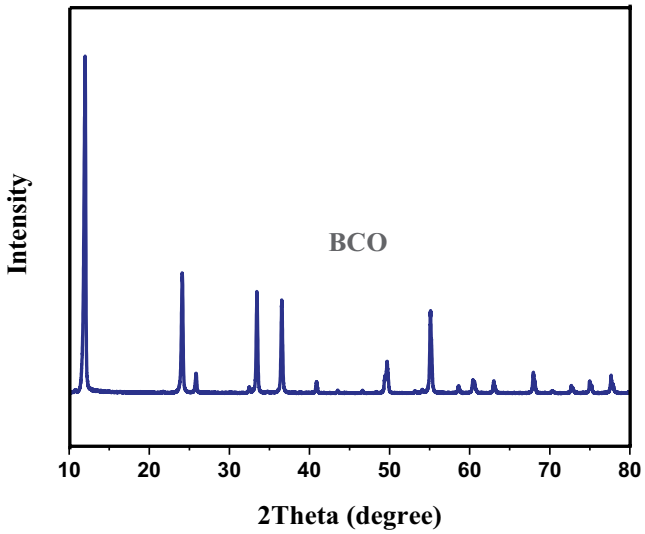

Fig. 3. X-ray diffraction pattern $BaCO_3$ nanoparticles.

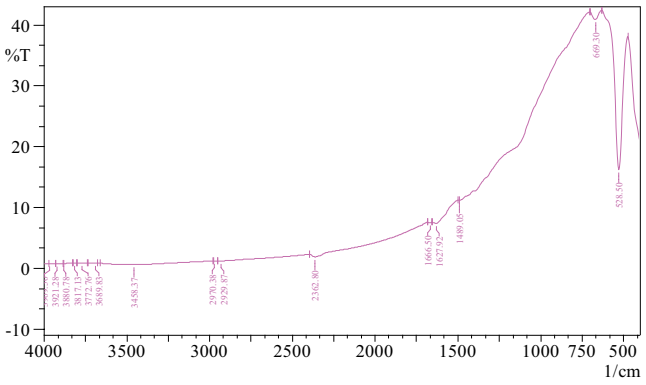

Fig. 4. X-ray diffraction pattern $BaCO_3$ nanoparticles.

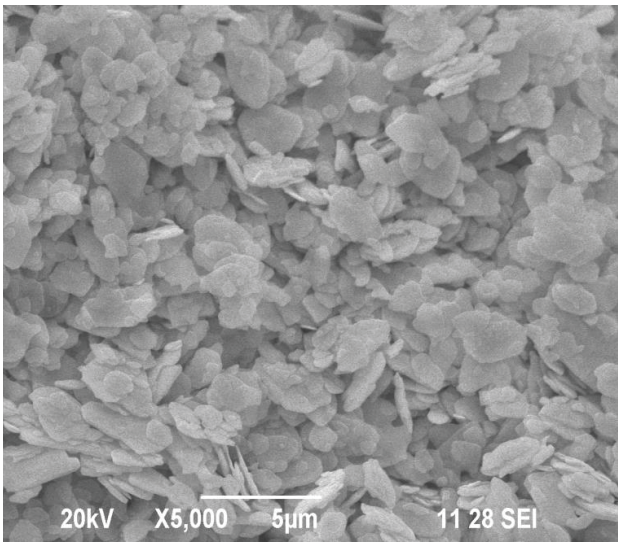

Fig. 5. Scanning electron microscopy image of BCO.

$$\ln\frac{C_0}{C} = kt + \ln\frac{C_0}{C} \quad (4)$$

where C_0 is the original concentration, C_1 is the concentration after adsorption, C is the concentration at different irradiation time of CV and k is the pseudo-first-order rate constant.

3.6. Photocatalytic reaction

The photocatalytic exercises of BCO were tried by CV (10 μM) debasement under obvious light illumination in a mechanical assembly [35]. Obvious light (420 < 1 < 800 nm) created by a 500 W Xe light outfitted with two optical channels was utilized as the light source. The force thickness of obvious light at the situation of reactor was around 7.4 mW/cm^2 and the impetus content was 0.1 g/300 mL. Preceding light, the suspensions were attractively mixed in dull for 30 min. During the CV photodecomposition, tests were pulled back at normal spans and centrifuged to isolate strong particles for examination. The centralization of the CV was controlled by an UV-Vis spectroscopy at its greatest ingestion frequency around 554 nm [36].

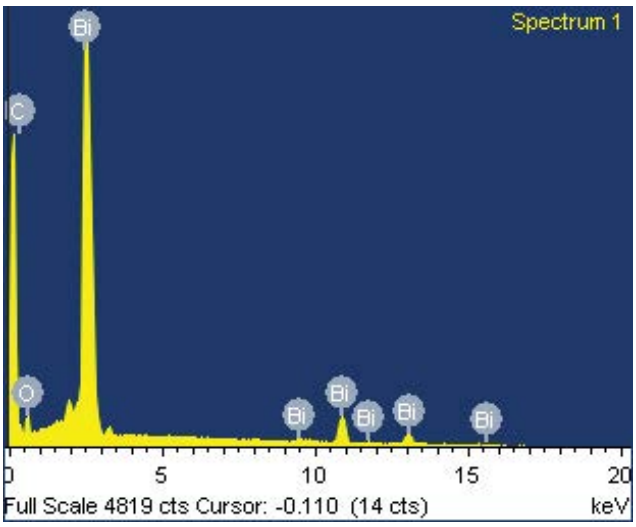

Fig. 6. Energy-dispersive X-ray spectroscopy image of BCO.

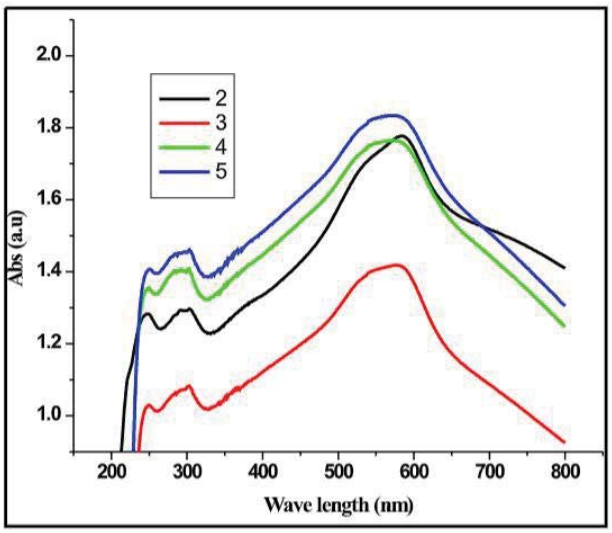

Fig. 7. Photocatalytic reaction of Crystal violet of BCO nanoparticles.

3.7. Photocatalytic degradation of Crystal violet

The photocatalytic action of BCO for the corruption of CV 10 μM and impetus fixation 0.1 g/300 mL. The outcomes uncovered that the debasement of Crystal violet is just accomplished in the nearness and the most elevated photocatalytic movement is appeared by BCO (91%). The photodegradation of CV was additionally done without light (just impetus) up to 150 min. The adsorption level of Crystal violet at 150 min of contact time is insignificant without nanocomposites. The most elevated photocatalytic movement of BCO can be clarified as follows. When the photocatalyst is illuminated by noticeable light, electrons and openings are shaped in conduction band and valence band of BCO (restricted band hole semiconductor). Thusly, productive electron-opening detachment is accomplished on the photocatalyst surface. The electron responds with surface

adsorbed O_2 to deliver $O_2^{\bullet-}$ and gaps respond with H_2O to make $^{\bullet}OH$. This outcome in more charge transporter to frame receptive species, which advance the degradation of CV.

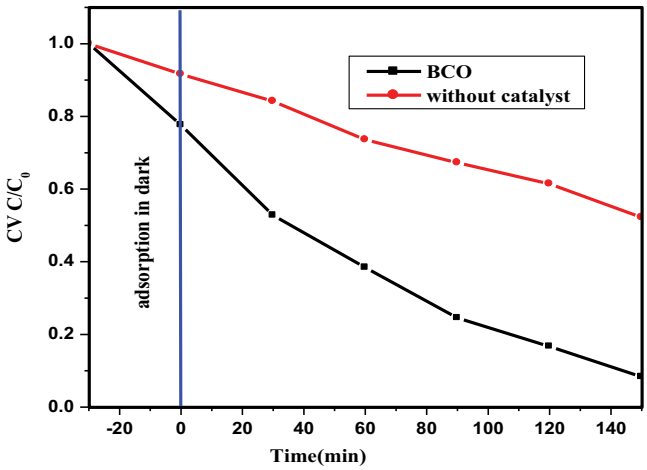

Fig. 8. Photodegradation of Crystal violet in the presence of BCO.

3.8. Kinetics and mechanism of photodegradation of Crystal violet

The kinetics of photodegradation of CV was studied by conducting the experiments under optimum operation conditions (Crystal violet concentration 10 μM, BCO concentration 0.1 g/300 mL and irradiation time 150 min). In all experiments, the degradation followed first order kinetics (plots of $-\ln[C/C_0]$ vs. time showed linear relationship, where C is the concentration of CV remaining in the solution at irradiation time of t, and C_0 is the initial concentration. First order rate constant were evaluated from the slopes of the $-\ln[C/C_0]$ vs. time plots (Fig. 9). The observed rate constant for the photodegradation of Crystal violet in the presence of BCO is 0.0061 min^{-1}.

3.9. Effect of catalyst dosage

The response rate as a component of impetus focus is imperative to survey the measure of BCO impetus required. Trials were performed utilizing shifted impetus levels in the scope of 0.1–0.4 g/300 mL at a fixed centralization of 10 μM/L of CV and the debasement time was additionally fixed as 180 min [37]. The centralization of the photocatalyst is found to impact the corruption of Crystal violet as

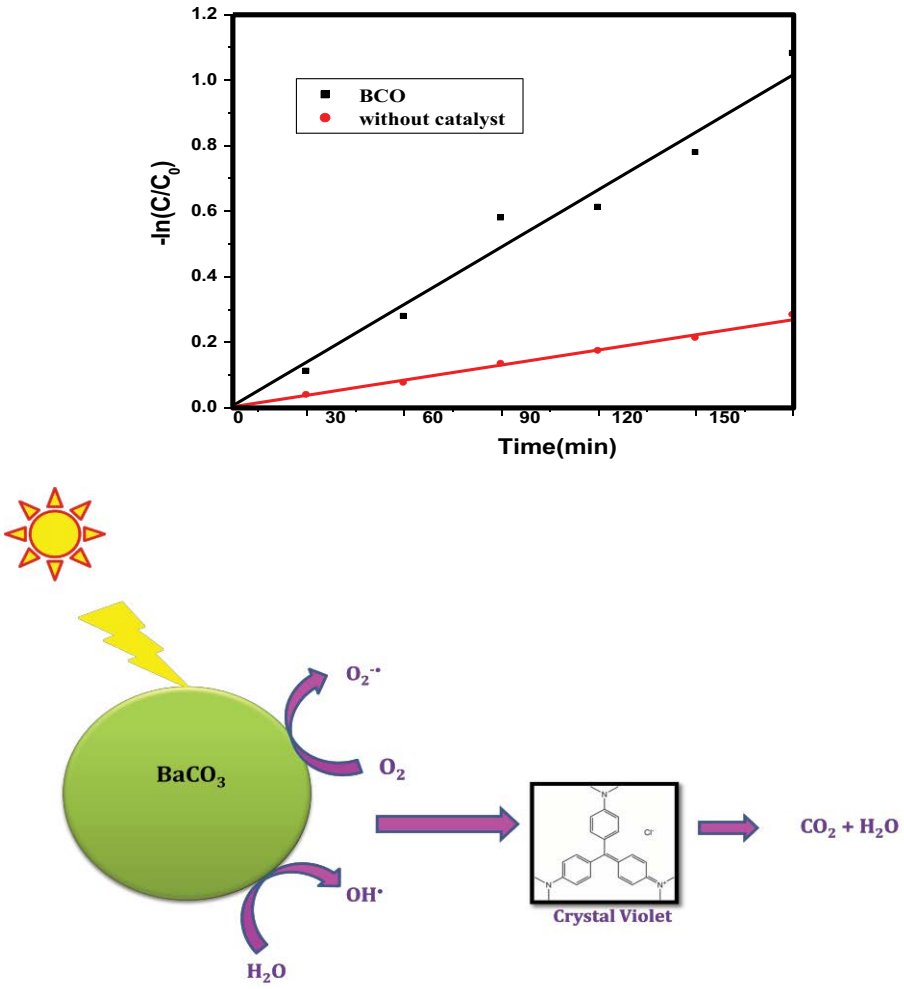

Fig. 9. Kinetics regime and mechanism on the photodegradation of Crystal violet in the presence of BCO.

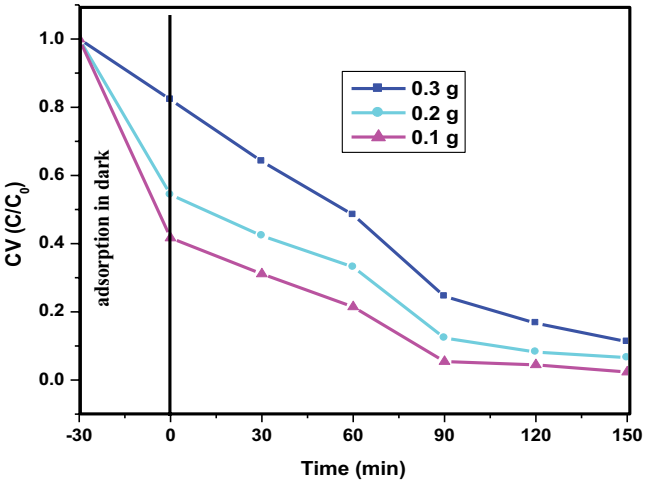

Fig. 10. Effect of catalyst dosage on photodegradation of Crystal violet.

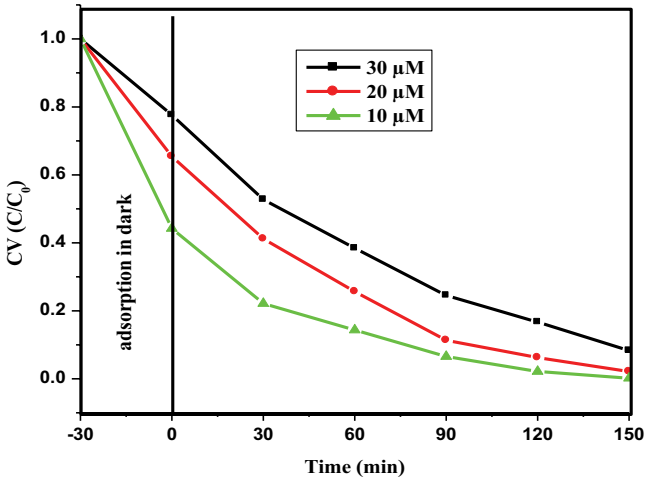

Fig. 11. Effect of concentration of Crystal violet and its photodegradation.

Table 1
Fourier-transform infrared spectroscopy values of BCO

S. No.	$BaCO_3$	Assignments
1	528.3 and 669.3	In plane bending CO_3
2	1,489	Asymmetric C–O stretching vibration

Table 2
Energy-dispersive X-ray spectroscopy analysis of BCO

S. No.	Element	KeV
1	Ba	1.17
2	C	1.04
3	O	0.79

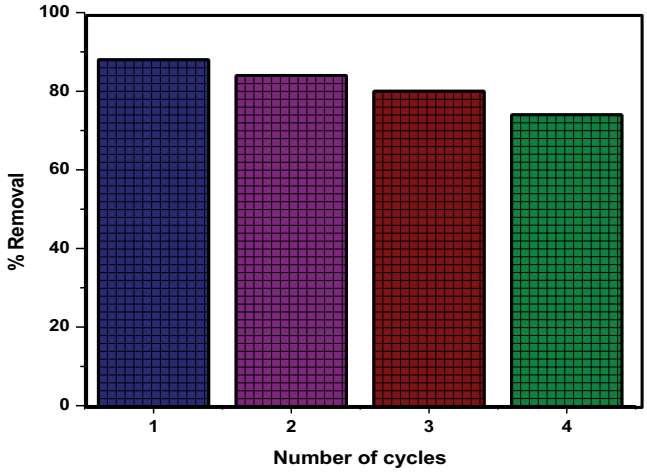

Fig. 12. Reusability and recyclability of BCO.

appeared in Fig. 10. It is accounted for that the impetus fixation has both a positive and negative effect on the photodegradation rate and the abundance impetus forestalls the arrangement of the OH, an essential oxidant in the photocatalytic framework, in this manner diminishing the productivity of the corruption appropriately. As a result of this, some portion of the impetus surface gets inaccessible for photon assimilation and thus, the debasement rate diminishes. Be that as it may, for high impetus dose, the turbidity increments. This impact suggests that the accessibility of dynamic destinations diminishes with expanding color focus [38].

3.10. Effect of dye concentration

It is uncovered from the watched outcomes that the underlying color fixation impacts the corruption pace of the due [39]. As the underlying convergence of color expands, the debasement rate diminishes. Results show that a fixed fixation 0.1 g/300 mL of BCO can be utilized for CV color corruption in the focus scope of 10–30 µM. At high color focus, a lot of light might be consumed by the color atoms as opposed to the impetus which may likewise diminish the photocatalytic rate [40]. As the underlying grouping of Crystal violet builds, the corruption likewise increments. Therefore, the corruption pace of the color diminishes with the expansion in the color focus as appeared in Fig. 11. In such cases the OH. Furthermore, $O_2^{\bullet-}$ framed on the outside of the photograph impetus are likewise steady, so the quality of OH. What's more, $O_2^{\bullet-}$ vs. expanding convergence of colors become less accordingly diminishing the photodegradation proficiency [41]. Henceforth the optimum grouping of CV for improved photograph synergist corruption is seen as 10 µM.

3.11. Reusability and recyclability of BCO

Reusability and recyclability are the important characteristics of the photocatalyst to be used for practical applications [42–44]. The percentage of removal after first cycle - 88%, second cycle - 84%, third cycle - 80% and fourth cycle - 78%, respectively. After the completion of the reaction cycle, the catalyst was isolated by suction filtration using Whatman filter paper, washed with ethanol followed

by an excess of double-distilled water and dried. The dried catalyst was then used for the next cycle of the photocatalytic reduction with fresh substrates. More efficient transfer and improved catalytic activity can be achieved even after five cycles, as shown in Fig. 12.

4. Conclusion

In this current work, $BaCO_3$ has been effectively combined and viably used for noticeable light determined photocatalyst for the corruption of precious stone violet. The readied nanoparticles have been described utilizing UV-Vis DRS, FT-IR, XRD, SEM, and EDX procedure. From the consequences of XRD the littlest molecule size and as well as can be expected be watched for the $BaCO_3$ acquired at 30.8 nm. Likewise additional proof for the immaculateness and stoichiometry of the item was acquired by EDX ranges, individually. In correlation with some different techniques revealed for arrangement of $BaCO_3$ nanoparticles, this work shows generally an advantageous and minimal effort course for the enormous scope amalgamation of this nano-scale item with a little size. $BaCO_3$ (91%) shows higher photocatalytic action. The consequence of this examination work might be utilized for the barium carbonate nanoparticles.

Acknowledgement

Authors would like to thank the management of Cardamom Planters' Association College, Bodinayakanur and D.K.M. College for Women, Vellore for giving the necessary facilities to do this work.

Conflict of interest

There are no conflicts to declare.

References

[1] L. Zhang, K.H. Wong, Z. Chen, J.C. Yu, J. Zhao, C. Hu, Y.C. Chan, P.K. Wong, AgBr-Ag-Bi_2WO_6 nanojunction system: a novel and efficient photocatalyst with double visible-light active components, Appl. Catal., A, 363 (2009) 221–229.
[2] H. Chen, J. Zhao, Adsorption study for removal of Congo red anionic dye using organo-attapulgite, Adsorption, 15 (2009) 381–389.
[3] S.T. Ong, P.S. Keng, W.N. Lee, S.T. Ha, Y.T. Hung, Dye waste treatment, Water, 3 (2011) 157–176.
[4] S.H. Huo, X.P. Yan, Metal–organic framework MIL-100(Fe) for the adsorption of malachite green from aqueous solution, J. Mater. Chem., 22 (2012) 7449–7455.
[5] G. Crini, Non-conventional low-cost adsorbents for dye removal: a review, Bioresour. Technol., 97 (2006) 1061–1085.
[6] I.K. Konstantinou, T.A. Albanis, TiO_2 assisted photocatalytic degradation of azo dyes in aqueous solution: kinetic and mechanistic investigations: a review, Appl. Catal., B, 49 (2004) 1–14.
[7] A.K. Vera, R.R. Dash, P. Bhunia, A review on chemical coagulation/flocculation technologies for removal of colour from textile wastewaters, J. Environ. Manage., 93 (2012) 154–168.
[8] L.S. Andrade, L.A.M. Ruotolo, R.C. Rocha-Filho, N. Bocchi, S.R. Biaggio, J. Iniesta, V. García-Garcia, V. Montiel, On the performance of Fe and Fe,F doped Ti–Pt/PbO_2 electrodes in the electrooxidation of the Blue Reactive 19 dye in simulated textile wastewater, Chemosphere, 66 (2007) 2035–2043.
[9] C.I. Pearce, J. Lloyd, J. Guthrie, The removal of colour from textile wastewater using whole bacterial cells: a review, Dyes Pigm., 58 (2003) 179–196.
[10] V.K. Gupta, A. Mittal, R. Jain, M. Mathur, S. Sikarwar, Adsorption of Safranin-T from wastewater using waste materials-activated carbon and activated rice husks, J. Colloid Interface Sci., 303 (2006) 80–86.
[11] S.K. Alpat, O. Ozbayrak, S. Alpat, Akçay, The adsorption kinetics and removal of cationic dye, Toluidine Blue O, from aqueous solution with Turkish zeolite, J. Hazard. Mater., 151 (2008) 213–220.
[12] X. Lu, W. Yang, Z. Quan, T. Lin, L. Bai, L. Wang, F. Huang, Y. Zhao, Enhanced electron transport in Nb-doped TiO_2 nanoparticles *via* pressure-induced phase transitions, J. Am. Chem. Soc., 136 (2014) 419–426.
[13] B. Ohtani, Photocatalysis A to Z–what we know and what we do not know in a scientific sense, J. Photochem. Photobiol., C, 11 (2010) 157–178.
[14] T.L. Thompson, J.T. Yates, Surface science studies of the photoactivation of TiO_2 – new photochemical processes, Chem. Rev., 106 (2006) 4428–4453.
[15] D. Chen, K. Wang, W. Hong, R. Zong, W. Yao, Y. Zhu, Visible light photoactivity enhancement via CuTCPP hybridized g-C_3N_4 nanocomposite, Appl. Catal., B, 166 (2015) 366–373.
[16] S.B. Zhu, T.G. Xu, H.B. Fu, J. Zhao, Y. Zhu, Synergetic effect of Bi_2WO_6 photocatalyst with C_{60} and enhanced photoactivity under visible irradiation, Environ. Sci. Technol., 41 (2007) 6234–6239.
[17] Y. Wang, X. Bai, C. Pan, J. He, Y. Zhu, Enhancement of photocatalytic activity of Bi_2WO_6 hybridized with graphite-like C_3N_4, J. Mater. Chem., 22 (2012) 11568–11573.
[18] S. Chen, Y. Hu, X. Jiang, S. Meng, X. Fu, Fabrication and characterization of novel Z-scheme photocatalyst WO_3/g-C_3N_4 with high-efficient visible light photocatalytic activity, Mater. Chem. Phys., 149–150 (2015) 512–521.
[19] N. Tian, H. Huang, Y. Guo, Y. He, Y. Zhang, A g-C_3N_4/$Bi_2O_2CO_3$ composite with high visible-light-driven photocatalytic activity for Rhodamine B degradation, Appl. Surf. Sci., 322 (2014) 249–254.
[20] Y.T. Liang, B.K. Vijayan, K.A. Gray, M.C. Hersam, Minimizing graphene defects enhances titania nanocomposite based photocatalytic reduction of CO_2 for improved solar fuel production, Nano Lett., 11 (2011) 2865−2870.
[21] Q.P. Luo, X.Y. Yu, B.X. Lei, H.Y. Chen, D.B.C. Kuang, Y. Su, Reduced graphene oxide-hierarchical ZnO hollow sphere composites with enhanced photocurrent and photocatalytic activity, J. Phys. Chem. C, 116 (2012) 8111−8117.
[22] F. Cai, Y. Tang, F. Chen, Y. Yan, W. Shi, Enhanced visible-light-driven photocatalytic degradation of tetracycline by Cr^{3+} doping $SrTiO_3$ cubic nanoparticles, RSC Adv., 5 (2015) 21290–21296.
[23] C.A. Bignozzi, S. Caramori, V. Cristino, R. Argazzi, L. Meda, A. Tacca, Nanostructured photoelectrodes based on WO_3: applications to photooxidation of aqueous electrolytes, Chem. Soc. Rev., 42 (2013) 2228–2246.
[24] V. Fischer, M.B. Bannwarth, G. Jakob, K. Landfester, R. Munoz-Espi, Luminescent and magnetoresponsive multifunctional chalcogenide/polymer hybrid nanoparticles, J. Phys. Chem. C, 117 (2013) 5999–6005.
[25] V. Purushothaman, S. Prabhu, K. Jothivenkatachalam, S. Parthiban, J.Y. Kwon, K. Jeganathan, Photocatalytic dye degradation properties of wafer level GaN nanowires by catalytic and self-catalytic approach using chemical vapor deposition, RSC Adv., 4 (2014) 25569–25575.
[26] Z. Zhang, W. Wang, M. Shang, W. Yin, Photocatalytic degradation of Rhodamine B and phenol by solution combustion synthesized $BiVO_4$ photocatalyst, Catal. Commun., 11 (2010) 982–986.
[27] K. Yu, S. Yang, H. He, C. Sun, C. Gu, Y. Ju, Visible light-driven photocatalytic degradation of Rhodamine B over $NaBiO_3$: pathways and mechanism, J. Phys. Chem. A, 113 (2009) 10024–10032.
[28] B. Chai, J. Li, Q. Xu, Reduced graphene oxide grafted Ag_3PO_4 composites with efficient photocatalytic activity under visible-light irradiation, Ind. Eng. Chem. Res., 53 (2014) 8744−8752.

[29] R. Verma, S.K. Samdarshi, *In-situ* decorated optimized CeO_2 on reduced graphene oxide with enhanced adsorptivity and visible light photocatalytic stability and reusability, J. Phys. Chem. C, 120 (2016) 22281–22290.
[30] L. Whittaker-Brooks, J. Gao, A.K. Hailey, C.R. Thomas, N. Yao, Y.L. Loo, Bi_2S_3 nanowire networks as electron acceptor layers in solution-processed hybrid solar cells, J. Mater. Chem. C, 3 (2015) 2686–2692.
[31] M. Barroso, S.R. Pendlebury, A.J. Cowan, J.R. Durrant, Charge carrier trapping, recombination and transfer in hematite (α-Fe_2O_3) water splitting photoanodes, Chem. Sci., 4 (2013) 2724–2734.
[32] G. Palmisano, E. Garcia-Lopez, G. Marci, V. Loddo, S. Yurdakal, V. Augugliaro, L. Palmisano, Advances in selective conversions by heterogeneous photocatalysis, Chem. Commun., 46 (2010) 7074–7089.
[33] H. Xeuli, L. Peng, H. Youzhou, W. Cheng, Anionic/cationic synergistic action of insulator $BaCO_3$ enhanced the photocatalytic activities of graphitic carbon nitride, Appl. Surf. Sci., 528 (2020) 146924, doi: 10.1016/j.apsusc.2020.146924.
[34] J.F. Huang, F.H. Tao, C.H. Yu, Y.J. Mao, Z.Y. Xue, M.C. Wang, C.G. Fan, L.Z. Pei, Hydrothermal synthesis and photocatalytic performance of barium carbonate/tin dioxide nanoparticles, Micro Nanosyst., 14 (2022) 204–211.
[35] X. Lv, W. Wei, Q. Sun, F. Li, B. Huang, Y. Dai, Two-dimensional germanium monochalcogenides for photocatalytic water splitting with high carrier mobility, Appl. Catal., B, 217 (2017) 275–284.
[36] A.D. Liyanage, S.D. Perera, K. Tan, Y. Chabal, K.J. Balkusjr, Synthesis, characterization, and photocatalytic activity of Y-doped CeO_2 nanorods, ACS Catal., 4 (2014) 577–584.
[37] Z. Zhang, S. Zhai, M. Wang, H. Ji, L. He, C. Ye, C. Wang, S. Fang, H. Zhang, Photocatalytic degradation of Rhodamine B by using a nanocomposite of cuprous oxide, three-dimensional reduced graphene oxide, and nanochitosan prepared via one-pot synthesis, J. Alloys Compd., 659 (2016) 101–111.
[38] Y. Wang, W. Wang, H. Mao, Y. Lu, J. Lu, J. Huang, Z. Ye, B. Lu, Electrostatic self-assembly of $BiVO_4$–reduced graphene oxide nanocomposites for highly efficient visible light photocatalytic activities, ACS Appl. Mater. Interfaces, 6 (2014) 12698–12706.
[39] J. Ding, W. Yan, S. Sun, J. Bao, C. Gao, Hydrothermal synthesis of $CaIn_2S_4$-reduced graphene oxide nanocomposites with increased photocatalytic performance, ACS Appl. Mater. Interfaces, 6 (2014) 12877–12884.
[40] S. Liu, J. Tian, L. Wang, Y. Luo, X. Sun, One-pot synthesis of CuO nano flower decorated reduced graphene oxide and its application to photocatalytic degradation of dyes, Catal. Sci. Technol., 2 (2012) 339–344.
[41] C. Zhang, L. Ai, J. Jiang, Graphene hybridized photoactive iron terephthalate with enhanced photocatalytic activity for the degradation of Rhodamine B under visible light, Ind. Eng. Chem. Res., 54 (2015) 153–163.
[42] S. Issarapanacheewina, K. Wetchakun, S. Phanichphant, W. Kangwansupamonkon, N. Wetchakun, Efficient photocatalytic degradation of Rhodamine B by a novel CeO_2/Bi_2WO_6 composite film, Catal. Today, 278 (2016) 280–290.
[43] R. Arunadevi, B. Kavitha, M. Rajarajan, A. Suganthi, Sonochemical synthesis and high-efficient solar-light-driven photocatalytic activity of novel cobalt and manganese co-doped tungsten oxide nanoparticles, Chem. Phys. Lett., 715 (2019) 252–262.
[44] R. Arunadevi, B. Kavitha, M. Rajarajan, A. Suganthi, Synthesis of Ce/Mo-V_4O_9 nanoparticles with superior visible light photocatalytic activity for Rhodamine-B degradation, J. Environ. Chem. Eng., 6 (2018) 3349–3357.